different edges on top of the monotonously decaying background is a signature of the elemental composition, the intensity of the signals being roughly proportional to the relative concentration in the associated element. Core-level EELS spectroscopy therefore investigates transitions from one well defined atomic orbital to a vacant state above the Fermi level: it is a probe of the energy distribution of vacant states in a solid, see Fig. 4.3.4.5. As the excited electron is promoted on a given atomic site, the information involved has two specific characters: it provides the local atomic point of view and it reflects the existence of the hole created, which can be more or less screened by the surrounding population of electrons in the solid. The properties of this family of excitations are the subject of Subsection 4.3.4.4.

The non-characteristic background is due to the superposition of several contributions: the high-energy tail of valence-electron scattering, the tails of core losses with lower binding energy, *Bremsstrahlung* energy losses, plural scattering, *etc*. It is therefore rather difficult to model its behaviour, although some efforts have been made along this direction using Monte Carlo simulation of multiple scattering (Jouffrey, Sevely, Zanchi & Kihn, 1985).

When one monochromatizes the natural energy width of the primary beam to much smaller values (about a few meV) than its natural width, one has access to the infrared part of the electromagnetic spectrum. An example is provided in Fig. 4.3.4.6 for a specimen of germanium in the energy-loss range 0 up to 500 meV. In this case, one can investigate phonon modes, or the bonding states of impurities on surfaces. This field has been much less extensively studied than the higher-energy-loss range [for references see Ibach & Mills (1982)].

Generally, EELS techniques can be applied to a large variety of specimens. However, for the following review to remain of limited size, it is restricted to electron energy-loss spectroscopy on solids and surfaces in transmission and reflection. It omits some important aspects such as electron energy-loss spectroscopy in gases with its associated information on atomic and molecular states. In this domain, a bibliography of inner-shell excitation studies of atoms and molecules by electrons, photons or theory is available from Hitchcock (1982).

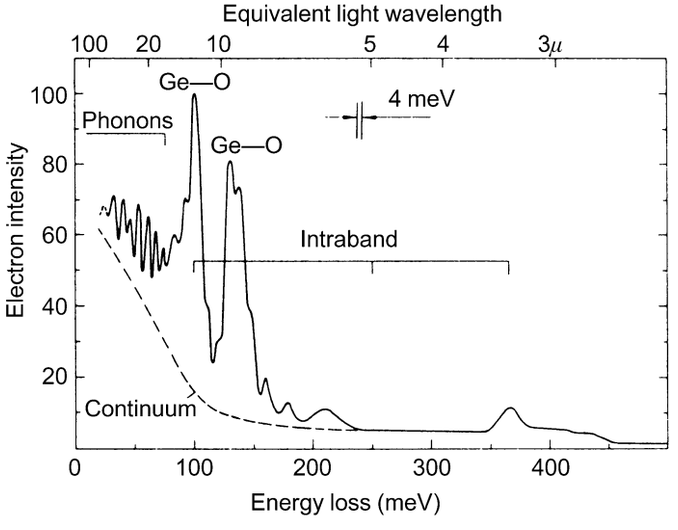

Fig. 4.3.4.6. Energy-loss spectrum, in the meV region, of an evaporated germanium film (thickness $\simeq 25$ nm). Primary electron energy 25 keV. Scattering angle $< 10^{-4}$. One detects the contributions of the phonon excitation, of the Ge—O bonding, and of intraband transitions [courtesy of Schröder & Geiger (1972)].

Table 4.3.4.1. *Different possibilities for using EELS information as a function of the different accessible parameters* (**r**, θ, ΔE)

	Integration parameter	Selection parameter	Results	Working mode of the spectrometer
1	**θ**	**r**	Spectrum $I_{\mathbf{r}}$ (ΔE)	Analyser
2	**r**	**θ**	Spectrum $I_{\boldsymbol{\theta}}$ (ΔE)	Analyser
3	**θ**	ΔE	Energy-filtered image $I_{\Delta E}(\mathbf{r})$	Filter
4	**r**	ΔE	Energy-filtered diffraction pattern $I_{\Delta E}(\boldsymbol{\theta})$	Filter

4.3.4.2. *Instrumentation*

4.3.4.2.1. *General instrumental considerations*

In a dedicated instrument for electron inelastic scattering studies, one aims at the best momentum and energy resolution with a well collimated and monochromatized primary beam. This is achieved at the cost of poor spatial localization of the incident electrons and one assumes the specimens to be homogeneous over the whole irradiated volume. In a sophisticated instrument such as that built by Fink & Kisker (1980), the energy resolution can be varied from 0.08 to 0.7 eV, and the momentum transfer resolution between 0.03 and 0.2 Å^{-1}, but typical values for the electron-beam diameter are about 0.2 to 1 mm. Nowadays, many energy-analysing devices are coupled with an electron microscope: consequently, an inelastic scattering study involves recording for a primary intensity I_0, the current $I(\mathbf{r}, \boldsymbol{\theta}, \Delta E)$ scattered or transmitted at the position **r** on the specimen, in the direction **θ** with respect to the primary beam, and with an energy loss ΔE. Spatial resolution is achieved either with a focused probe or by a selected area method, angular acceptance is defined by an aperture, and energy width is controlled by a detector function after the spectrometer. It is not possible from signal-to-noise considerations to reduce simultaneously all instrumental widths to very small values. One of the parameters (**r**, **θ** or ΔE) is chosen for signal integration, another for selection, and the last is the variable. Table 4.3.4.1. classifies these different possibilities for inelastic scattering studies.

Because of the great variety of possible EELS experiments, it is impossible to build an optimum spectrometer for all applications. For instance, the design of a spectrometer for low-energy incident electrons and surface studies is different from that for high-energy incident electrons and transmission work. In the latter category, instruments built for dedicated EELS studies (Killat, 1974; Gibbons, Ritsko & Schnatterly, 1975; Fink & Kisker, 1980; *etc*.) are different from those inserted within an electron-microscope environment, in which case it is possible to investigate the excitation spectrum from a specimen area well characterized in image and diffraction [see the reviews by Colliex (1984) and Egerton (1986)].

The literature on dispersive electron–optical systems (equivalent to optical prisms) is very large. For example, the theory of uniform field magnets, which constitute an important family of analysing devices, has been extensively developed for the components in high-energy particle accelerators (Enge, 1967; Livingood, 1969). As for EELS spectrometers, they can be classified as:

(*a*) *Monochromators*, which filter the incident beam to obtain the smallest primary energy width. The natural width for a heated W filament is about 1 eV, possibly rising to about a few eV as a consequence of stochastic interactions [Boersch (1954) effect, analysed for instance by Rose & Spehr (1980)]. For a low-temperature field-emission source, this energy spread is only ~0.3 eV. This constitutes a clear gain but remains insufficient for meV studies. In this case, one has to introduce a filter lens such as the three-electrode design developed by Hartl (1966) or a cylindrical electrostatic deflector before the accelerator [Kuyatt & Simpson (1967) or Gibbons *et al.* (1975)]. In both cases, an energy resolution of 50 meV has been achieved for electron beams of 50–300 keV at the specimen.

(*b*) *Analysers*, which measure the energy distribution of the beam scattered from the specimen. They can be used either strictly as analysers displaying the energy loss from a given specimen volume, or as filters (or selecting devices) that provide 2D images or diffraction patterns with a given energy loss.

4.3.4.2.2. *Spectrometers*

Fig. 4.3.4.7 defines the basic parameters of a 'general' energy-loss spectrometer: a region of electrostatic **E** and/or magnetic **B** fields transforms a distribution of electrons I_0 $(x_0, y_0, t_0, u_0, \rho)$ in the object plane of coordinate z_0 along the principal trajectory, into a distribution of electrons I_1 $(x_1, y_1, t_1, u_1, \rho)$ in the object plane of coordinate z_1, coincident with the detector plane (or optically conjugate to it). The transverse coordinates are labelled as (x, y), the angular ones as (t, u), and $\rho = \Delta p/p = \Delta E/2E$ is the relative change in absolute momentum value associated with the energy loss.

Common properties of such systems are:

(*a*) first-order imaging properties or stigmatism, *i.e.* all electrons leaving (x_0, y_0) are focused at the same (x_1, y_1) point, independently of their inclination on the optical axis;

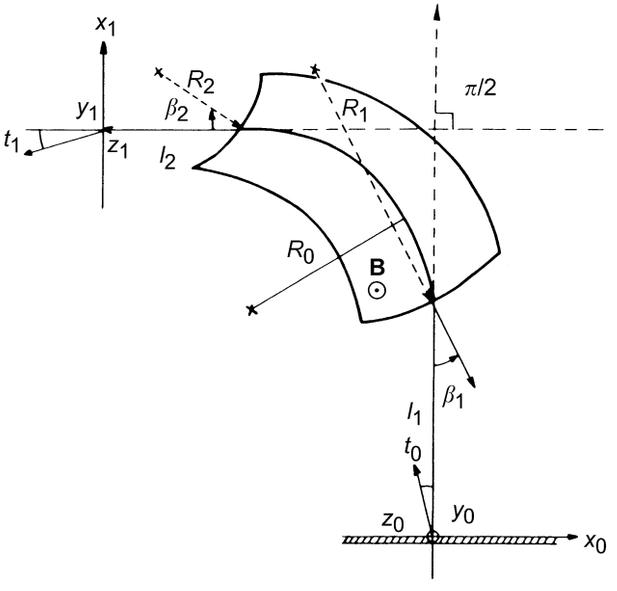

Fig. 4.3.4.7. Schematic drawing of a uniform magnetic sector spectrometer with induction **B** normal to the plane of the figure. Definition of the coordinates used in the text (the object plane at coordinate z_0 along the mean trajectory coincides with the specimen, and the image plane at z_1 coincides with the dispersion plane and the detector level).

(*b*) strong chromatic aberration in order to realize an efficient discrimination between electrons of different ρ.

The spectrometer performance can be evaluated with the following parameters:

D = *dispersion* = beam displacement in the spectrometer image plane for a given momentum change ρ; it is generally expressed in cm/eV. The higher the dispersion, the easier it is to resolve small energy losses. For a straight-edge 90° magnetic sector, $D \propto 2R/E_0$, where R is the curvature radius of the mean trajectory and E_0 is the primary energy.

$\delta E_{\min}$ = *energy resolution*. This corresponds to the minimum-energy variation that can be resolved by the instrument. It takes into account the width of the image $\Delta x_{\text{image}} = Mr$, where M is the spectrometer magnification and r the radius of the spectrometer source, as well as the second- and higher-order angular aberrations. These are responsible for the imperfect focusing of the electrons that enter the spectrometer within a cone of angular acceptance β_0 and contribute through a term $\Delta x_{\text{aber}} = C\beta_0^2$. Moreover, one must convolute these terms with the natural width δE_0 of the primary beam, including AC fields, and with the detection slit width Δx_{slit}. Combining all these effects, as shown schematically in Fig. 4.3.4.8, one obtains approximately:

$$\Delta x_{\text{tot}} = [(\Delta x_{\text{slit}})^2 + (\Delta x_{\text{image}})^2 + (\Delta x_{\text{aber}})^2 + D\delta E_0^2]^{1/2} \quad (4.3.4.7)$$

and the corresponding energy resolution is defined as $\delta E_{\min} = (\Delta x_{\text{tot}})_{\min}/D$. In many situations, the dominant factor is the second-order aberration term $C\beta_0^2$ so that the figure of merit F, defined as $F = \pi\beta_0 E_0/\delta E_{\min}$, is of the order of unity for an uncorrected magnetic spectrometer.

From this simplified discussion, one deduces that there is generally competition between large angular acceptance for the inelastic signal, which is very important for obtaining a high signal-to-noise ratio (SNR) for core-level excitations, and good energy resolution. Two solutions have been used to remedy this limitation. The first is to improve spectrometer design, for example by correcting second-order aberrations in a homogeneous magnetic prism (Crewe, 1977*a*; Parker, Utlaut & Isaacson, 1978; Egerton, 1980*b*; Krivanek & Swann, 1981; *etc*). This can enhance the figure of merit by at least a factor of 100. The second possibility is to transform the distribution of electrons to be analysed at the exit surface of the specimen into a more convenient distribution at the spectrometer entrance. This can be done by introducing versatile transfer optics (see Crewe, 1977*b*; Egerton, 1980*a*; Johnson, 1980; Craven & Buggy, 1981; *etc*.). As a final remark on the energy resolution of a spectrometer, it is meaningless to define it without reference to the size and the angular aperture of the analysed beam.

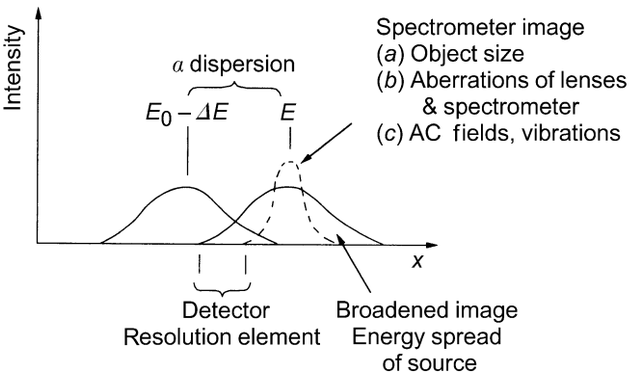

Fig. 4.3.4.8. Different factors contributing to the energy resolution in the dispersion plane [courtesy of Johnson (1979)].

Historically, many types of spectrometer have been used since the first suggestion by Wien (1897) that an energy analyser could be designed by employing crossed electric and magnetic fields. Reviews have been published by Klemperer (1965), Metherell (1971), Pearce-Percy (1978), and Egerton (1986). Nowadays, two configurations are mostly used and have become commercially available on modern electron microscopes: these are spectrometers on TEM/STEM instruments and filters on CTEM ones. In the first case, *homogeneous magnetic sectors* are the simplest and most widely used devices. Recent instrumental developments by Shuman (1980), Krivanek & Swann (1981), and Scheinfein & Isaacson (1984) have given birth to a generation of spectrometers with the following major characteristics: double focusing, correction for second-order aberrations, dispersion plane perpendicular to the trajectory. This has been made possible by a suitable choice of several parameters, such as the tilt angles and the radius of curvature for the entrance and exit faces and the correct choice of the object source position. As an example, for a 100 keV STEM equipped with a field emission gun, the coupling illustrated in Fig. 4.3.4.9 leads to an energy resolution of 0.35 eV for $\beta_0 = 7.5$ mrad on the specimen as visible on the elastic peak, and 0.6 eV for $\alpha_0 = 25$ mrad as checked on the fine structures on core losses. Krivanek, Manoubi & Colliex (1985) demonstrated a sub-eV energy resolution over the whole range of energy losses up to 1 or 2 keV.

A very competitive solution is the *Wien filter*, which consists of uniform electric and magnetic fields crossed perpendicularly, see Fig. 4.3.4.10. An electron travelling along the axis with a velocity $\mathbf{v}_0$ such that $|\mathbf{v}_0| = E/B$ is not deflected, the net force on it being null. All electrons with different velocities, or at some angle with respect to the optical axis, are deflected. The dispersion of the system is greatly enhanced by decelerating the electrons to about 100 eV within the filter, in which case $D \simeq$ a few 100 μm/eV. A presently achievable energy resolution of 150 meV at a spectrometer collection half-angle of 12.5 mrad has been demonstrated by Batson (1986, 1989). It allows the study of the detailed shape of the energy distribution of the electrons emitted from a field emission source and the taking of it into account in the investigation of band-gap states in semiconductors (Batson, 1987).

Filtering devices have been designed to form an energy-filtered image or diffraction pattern in a CTEM. The first

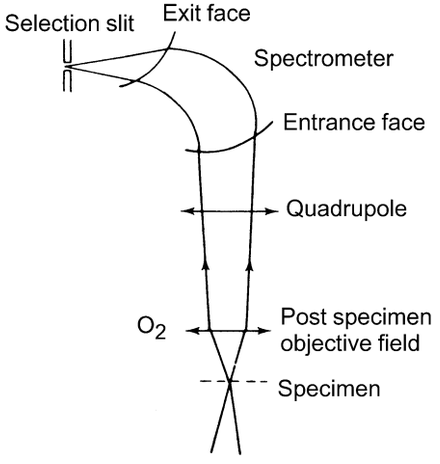

Fig. 4.3.4.9. Optical coupling of a magnetic sector spectrometer on a STEM column.

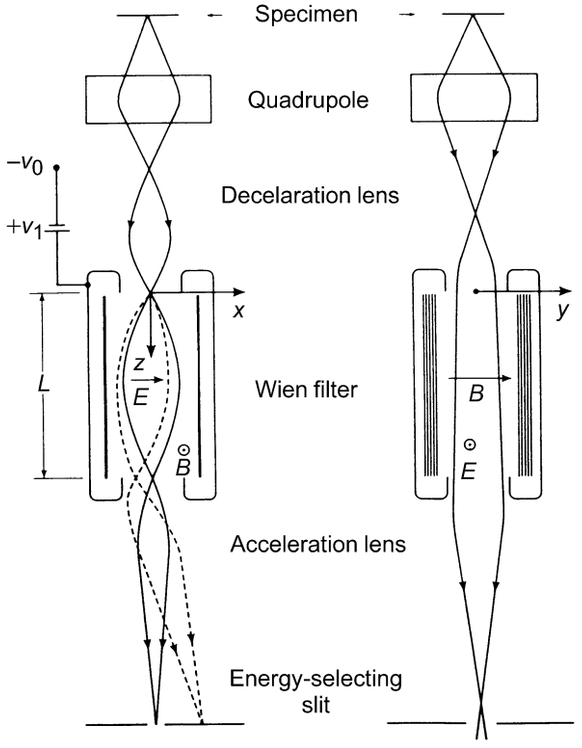

Fig. 4.3.4.10. Principle of the Wien filter used as an EELS spectrometer: the trajectories are shown in the two principal (dispersive and focusing) sections.

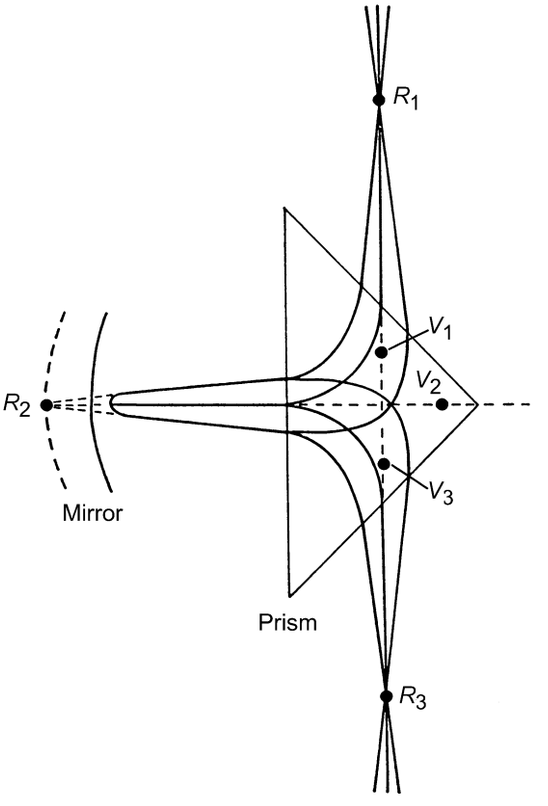

Fig. 4.3.4.11. Principle of the Castaing & Henry filter made from a magnetic prism and an electrostatic mirror. (R_1, R_2, and R_3 are the real conjugate stigmatic points, and V_1, V_2, and V_3 the virtual ones: the dispersion plane coincides with the R_3 level and achromatic one with the V_3 level.)

Table 4.3.4.2. *Plasmon energies measured (and calculated) for a few simple metals; most data have been extracted from Raether (1980)*

Monovalent			Divalent			Trivalent			Tetravalent		
	$\hbar\omega_p$ (eV)			$\hbar\omega_p$ (eV)			$\hbar\omega_p$ (eV)			$\hbar\omega_p$ (eV)	
	Meas.	Calc.		Meas.	Calc.		Meas.	Calc.		Meas.	Calc.
Li	7.1	(8.0)	Be	18.7	(18.4)	B	22.7	(?)	C	34.0	(31)
Na	5.7	(5.9)	Mg	10.4	(10.9)	Al	14.95	(15.8)	Si	16.5	(16.6)
K	3.7	(4.3)	Ca	8.8	(8.0)	Ga	13.8	(14.5)	Ge	16.0	(15.6)
Rb	3.4	(3.9)	Sr	8.0	(7.0)	In	11.4	(12.5)	Sn	13.7	(14.3)
Cs	2.9	(3.4)	Ba	7.2	(6.7)	Sc	14.0	(12.9)	Pb	(13)	(13.5)

solution, reproduced in Fig. 4.3.4.11, is due to Castaing & Henry (1962). It consists of a double magnetic prism and a concave electrostatic mirror biased at the potential of the microscope cathode. The system possesses two pairs of stigmatic points that may coincide with a diffraction plane and an image plane of the electron-microscope column. One of these sets of points is achromatic and can be used for image filtering. The other is strongly chromatic and is used for spectrum analysis. Zanchi, Sevely & Jouffrey (1977) and Rose & Plies (1974) have proposed replacing this system, which requires an extra source of high voltage for the mirror, by a purely magnetic equivalent device. Several solutions, known as the α and ω filters, with three or four magnets, have thus been built, both on very high voltage microscopes (Zanchi, Perez & Sevely, 1975) and on more conventional ones (Krahl & Herrmann, 1980), the latest version now being available from one EM manufacturer (Zeiss EM S12).

4.3.4.2.3. *Detection systems*

The final important component in EELS is the detector that measures the electron flux in the dispersion plane of the spectrometer and transfers it through a suitable interface to the data storage device for further computer processing. Until about 1990, all systems were operated in a sequential acquisition mode. The dispersed beam was scanned in front of a narrow slit located in the spectrometer dispersion plane. Electrons were then generally recorded by a combination of scintillator and photomultiplier capable of single electron counting.

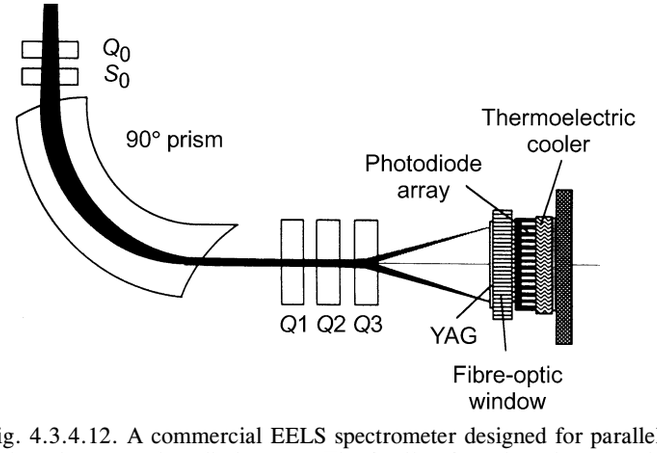

Fig. 4.3.4.12. A commercial EELS spectrometer designed for parallel detection on a photodiode array. The family of quadrupoles controls the dispersion on the detector level [courtesy of Krivanek *et al.* (1987))].

This process is, however, highly inefficient: while the counts are measured in one channel, all information concerning the other channels is lost. These requirements for improved detection efficiency have led to the consideration of possible solutions for parallel detection of the EELS spectrum. They use a multiarray of detectors, the position, the size and the number of which have to be adapted to the spectral distribution delivered by the spectrometer. In most cases with magnetic type devices, auxiliary electron optics has to be introduced between the spectrometer and the detector so that the dispersion matches the size of the individual detection cells. Different systems have been proposed and tested for recording media, the most widely used solutions at present being the photodiode and the charge-coupled diode arrays described by Shuman & Kruit (1985), Krivanek, Ahn & Keeney (1987), Strauss, Naday, Sherman & Zaluzec (1987), Egerton & Crozier (1987), Berger & McMullan (1989), *etc.* Fig. 4.3.4.12 shows a device, now commercially available from Gatan, that is made of a convenient combination of these different components. This progress in detection has led to significant improvements in many areas of EELS: enhanced detection limits, reduced beam damage in sensitive materials, data of improved quality in terms of both SNR and resolution, and access to time-resolved spectroscopy at the ms time scale (chronospectra). Several of these important consequences are illustrated in the following sections.

4.3.4.3. *Excitation spectrum of valence electrons*

Most inelastic interaction of fast incident electrons is with outer atomic shells in atoms, or in solids with valence electrons (referred to as conduction electrons in metals). These involve excitations in the 0–50 eV range, but, in a few cases, interband transitions from low-binding-energy shells may also contribute.

4.3.4.3.1. *Volume plasmons*

The basic concept introduced by the many-body theory in the interacting free electron gas is the volume plasmon. In a condensed material, the assembly of loosely bound electrons behaves as a plasma in which collective oscillations can be induced by a fast external charged particle. These eigenmodes, known as *volume plasmons*, are longitudinal charge-density fluctuations around the average bulk density in the plasma $n \simeq 10^{28}$ e^-/m^3). Their eigen frequency is given, in the free electron gas, as

$$\omega_p = \left(\frac{n e^2}{m\varepsilon_0}\right)^{1/2}. \qquad (4.3.4.8)$$

The corresponding $\hbar\omega_p$ energy, measured in an energy-loss spectrum (see the famous example of the plasmon in aluminium

references